Koroleva M.S., Piir I.V., Istomina E.I.
Chimica Techno Acta. 2017. Vol. 4, No. 4. P. 231–241.
ISSN 2409–5613

DOI: 10.15826/chimtech/2017.4.4.04

M.S. Koroleva, I.V. Piir, E.I. Istomina

Institute of Chemistry Komi SC UB RAS
48 Pervomayskaya St., Syktyvkar, 167982, Russian Federation
e-mail: marikorolevas@gmail.com

Synthesis, structure and electrical properties of Mg-, Ni-codoped bismuth niobates

Mg-, Ni-codoped bismuth niobates $Bi_{1.6}Mg_{0.8-x}Ni_xNb_{1.6}O_{7-\delta}$ (x = 0; 0.2; 0.4; 0.6; 0.8) were obtained by conventional solid-state reaction method. It was shown that the Mg atoms are distributed at the Nb sites while the Ni atoms are distributed over the Bi- and the Nb-sites, according to the results of comparison of pycnometric and X-ray density of the $Bi_{1.6}Mg_{0.4}Ni_{0.4}Nb_{1.6}O_{7-\delta}$ pyrochlore. In this case, about 15–20% of the vacancies are formed at the Bi sites. The obtained compounds are stable up to their melting point based on the DSC analysis data. Real dielectric permittivity ε' of the $Bi_{1.6}Mg_{0.8-x}Ni_xNb_{1.6}O_{7-\delta}$ samples decreases from 80 to 65 with the temperature decrease from 25 to 700 °C and practically does not depend on frequency in the range of 1–1000 kHz. Oxides $Bi_{1.6}Mg_{0.8-x}Ni_xNb_{1.6}O_{7-\delta}$ behave like insulators up to 280 °C, their conductivity increases with temperature ($E_{a,dc}$ ≈ 1.3 eV, dc) and with the Ni content at a given temperature.

Keywords: pyrochlore; $Bi_{1.6}Mg_{0.8-x}Ni_xNb_{1.6}O_{7-\delta}$; dopant distribution; dielectric behavior; electrical conductivity.

Received: 14.11.2017; accepted: 12.12.2017; published: 25.12.2017.

© Koroleva M.S., Piir I.V., Istomina E.I., 2017

Introduction

Ceramics in the Bi_2O_3-M_xO_y-Nb_2O_5 ternary system are interesting from the perspective of their dielectric properties. The most attention has been paid to the Zn-, Mg-containing bismuth niobates, which possess high dielectric constant (170–180) and low dielectric loss (~10^{-4}) at 1 MHz (at room temperature) [1–9]. To search for the same properties Fe- [10], Mn- [11–12], Co- [13], Ni- [12, 14–15], Cu- [12] and the mixed Zn-M (M – Sr [16], Ca [16–17], Mn [16, 18], Ti [19–22], Sn [19, 22], Zr [19, 21–22], Ce [19,22], Gd [21], Ta [23], La [24]), Mg-M (M – Sr [25], Nd [26], Cu [27]) bismuth niobates and other ones were synthesized. The improved permittivity was achieved by Ti doping of the Nb sites in the pyrochlore structure [21–22] and by Cu doping in $Bi_{1.5}Cu_xMg_{1-x}Nb_{1.5}O_7$ (x = 0.075) [27]. In most cases, doping leads to the permittivity decrease and to the tangent loss increase. However, electrical properties of several systems were investigated in the high temperature range (up to 700 °C) only in order to determine their conductivity mechanism [3, 9, 19–20, 27]. In our previous work [28–29] we have determined that the dielectric constant of the $Bi_{1.6}Cu_xMg_{0.8-x}Nb_{1.6}O_{7-\delta}$ pyrochlores behave

unusually passing through a maximum (250–350 °C) with temperature increasing. The value of the dielectric constant at the maximum is very high: ~10^6 (100 Hz). Second-type phase transition was found at 200 °C. To establish the reasons for such behavior, the distribution of doped metals in the cation (A–, B–sites) positions in the pyrochlore structure ($A_2B_2O_6O'$, the space group $Fd\bar{3}m$ (No 227)) was studied by X-ray diffraction pattern refinement (Rietveld analysis), and by comparison of pycnometric density with the calculated one. It has been determined that the electronegativity plays the crucial factor for the distribution of the Mg atoms in the Nb sites and the Cu atoms – in the Bi and the Nb sites in equal ratios. In any case, there are 10–15% of vacancies in the Bi sites. In accordance with the other systems' investigations, the vacancy concentration always remains at about 5–10% in the Bi sites in the pyrochlore structure [4, 10–11, 14, 30]. In this work we have a goal to determine a distribution of Ni and Mg dopants in the pyrochlore structure and investigate the temperature dependence of electrical properties of the $Bi_{1.6}Mg_{0.8-x}Ni_xNb_{1.6}O_{7-\delta}$.

Experimental

Mixed bismuth niobates $Bi_{1.6}Mg_{0.8-x}Ni_xNb_{1.6}O_{7-\delta}$ (x = 0; 0.2; 0.4; 0.6; 0.8) were prepared by a conventional solid state reaction method [31–32] from the oxides with high degree of purity (>99.9%): Bi_2O_3, NiO, MgO, Nb_2O_5. The oxides were weighted in an appropriate ratio (Bi_2O_3:MgO:NiO:Nb_2O_5 = 0.8:(0.8-x):x:0.8), grinded, pressed into pellets and calcined at 650 °C (8 h), 850 °C (6 h), 900 °C (6 h), 950 °C (12 h), 1000 °C (6 h), 1050 °C (12 h), 1070 (6 h), and 1100 °C (11 h) consequently in corundum crucibles. The annealing at 650 °C was carried out in order to avoid significant bismuth weight loss and the melting stage of Bi_2O_3 at 824 °C. As the temperature and duration of the calcination increased, the impurity phase content decreased. After each firing step, the pellets were regrinded for 30 min and repressed. The pellets' diameter and thickness varied from 12 to 14 mm and from 2.2 to 2.7 mm, respectively.

The phase composition of the samples was examined by powder X-ray diffraction method on a SHIMADZU XRD-6000 diffractometer using Cu Kα emission within the angle range 10–80° (the step – 0.05°). Distribution of nickel and magnesium atoms in the $Bi_{1.6}Mg_{0.4}Ni_{0.4}Nb_{1.6}O_{7-\delta}$ pyrochlore was determined by Rietveld analysis (FullProf software package [33]). Scanning electron microscopy (SEM) was carried out on a TESCAN VEGA 3 SBU microscope. The local composition of the samples was studied on polished pellets by energy dispersion spectroscopy (EDS). Differential scanning calorimetry (DSC) and thermogravimetric analysis (TG) of $Bi_{1.6}Mg_{0.4}Ni_{0.4}Nb_{1.6}O_{7-\delta}$ powder were carried out in the air in platinum crucibles with heating up to 1300 °C and a heating rate of 5 °C/min (NETZSCH STA 409 PC/PG). The electrical measurements were performed on the pellets, both sides of which were coated uniformly with a silver paste. Capacitance and dielectric loss tangent were measured by MT–4090 LCR meter in different gases (air, $p(O_2)$ = 0.21 atm and oxygen, $p(O_2)$ = 0.99 atm) at four frequencies (1, 10, 100, 200 kHz) in the temperature range of 25–750 °C. The impedance plots were measured by immittance meter E7-28 at 0.5 V in the temperature and frequency ranges 25–700 °C and 24 Hz – 10 MHz, respectively. The

electrical data were collected after 10 min after the thermal equilibrium was reached. The thermoelectric effect – Seebeck coefficient – was determined in the temperature range 130–330 °C in a temperature gradient of 30–40 °C across the material.

Results and discussion

Synthesis and Characterization

The XRD patterns of $Bi_{1.6}Mg_{0.8-x}Ni_xNb_{1.6}O_{7-\delta}$ ($0 \le x \le 0.8$) are shown in Fig. 1. The pyrochlore structure is formed for the $Bi_{1.6}Mg_{0.4}Ni_{0.4}Nb_{1.6}O_{7-\delta}$ composition only. The small amounts of second phases, identified as $MgNb_2O_6$ (*Pbcn* space group) and as $NiNb_2O_6$ (*Pbcn* space group), were found in the samples with $x = 0$; 0.2 and with $x = 0.6$; 0.8, respectively.

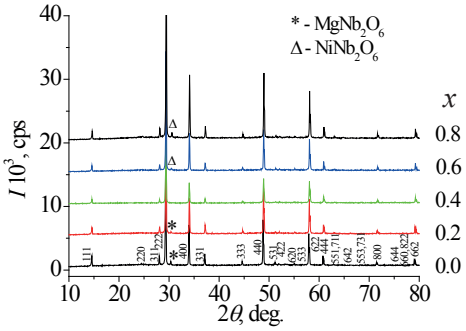

Fig. 1. X-ray diffraction patterns of $Bi_{1.6}Mg_{0.8-x}Ni_xNb_{1.6}O_{7-\delta}$ ($0 \le x \le 0.8$)

The surfaces of the $Bi_{1.6}Mg_{0.8-x}Ni_xNb_{1.6}O_{7-\delta}$ ($0 \le x \le 0.6$) polished pellets after the last calcination are shown in the SEM images (Fig. 2a–2c). According to the EDS data, the presence of additional phases such as $MgNb_2O_6$ (at $x = 0$) or as mixed Mg-Ni containing niobates (at $x = 0.2$; 0.6) can be seen. The amount of impurities is around 5%. The local compositions of the main and second phases are presented in the caption to Fig. 2. The composition of the $Bi_{1.6}Mg_{0.4}Ni_{0.4}Nb_{1.6}O_{7-\delta}$ ceramic determined by EDS is $Bi_{1.60}Mg_{0.38}Ni_{0.45}Nb_{1.6}O_{7-\delta}$, which is close to the desired composition. The porosity of the pellets was around 35–40%, as estimated from SEM micrographs.

DSC and TG curves of the $Bi_{1.6}Mg_{0.4}Ni_{0.4}Nb_{1.6}O_{7-\delta}$ powder are shown in Fig. 3. The endothermal effect was found on the DSC curve at 1261 °C. This effect may be associated with the melting of the sample. The reason for the weight rise during the heating process has not been established yet. It may be related to the partial oxidation of Ni^{+2} to Ni^{+3}.

The Rietveld refinement of the XRD pattern of $Bi_{1.6}Mg_{0.4}Ni_{0.4}Nb_{1.6}O_{7-\delta}$ was carried out. The occupations of atom sites were fixed in accordance with the quantitative composition of the compound. The possibility of displacement of the bismuth atoms (from 16*c* sites to 96*h* or 96*g* sites) and the oxygen atoms O′ associated with bismuth (from 8*a* sites to 32*e* sites) were considered, like in $[Bi_{0.833}Mg_{0.11}\square_{0.04}]_2[Mg_{0.24}Nb_{0.76}]_2O_7$ and in $[Bi_{0.833}Ni_{0.125}\square_{0.04}]_2[Ni_{0.25}Nb_{0.75}]_2O_7$ pyrochlores [14]. Various models were studied to determine the distribution of doped atoms in the cation (Bi, Nb) sites of the pyrochlore structure. Among the alternative models that were considered there are $[Bi_{1.56}Ni_{0.34}\square_{0.10}][Ni_{0.05}Mg_{0.39}Nb_{1.56}]O_{7.02}$ and $[Bi_{1.56}Mg_{0.34}\square_{0.10}][Mg_{0.05}Ni_{0.39}Nb_{1.56}]O_{7.02}$. In these models 5% of vacancies remain at the Bi sites. The distribution of dopant atoms in equal ratio among two different cation sites causes formation of about 2.5% vacant sites both in the Bi and Nb sublattices. It is not typical for the pyrochlore structure. The best agreement between theoretical and observed X-ray patterns was obtained for the model designated as

$[Bi_{1.56}Ni_{0.34}\square_{0.10}][Ni_{0.05}Mg_{0.39}Nb_{1.56}]O_{7.02}$. In this model, all Mg atoms are distributed over the Nb sites. Several models were considered with different vacancy concentrations (10–25%) in the Bi sites and Mg atoms occupying the Nb sites.

The best values of R_{wp} (%), R_p (%), χ^2 factors can be obtained for the models with 15–20% vacancies in the Bi sites. The refined crystallographic parameters of the $[Bi_{1.46}Ni_{0.18}\square_{0.36}][Ni_{0.18}Mg_{0.36}Nb_{1.46}]O_{6.52}$ model are presented in Table 1. This model corresponds to the equal distribution of Ni atoms in the Bi and the Nb sites, whereas 18% of vacancies remain in the Bi sites. Displacement of Bi and Ni atoms (16*c*

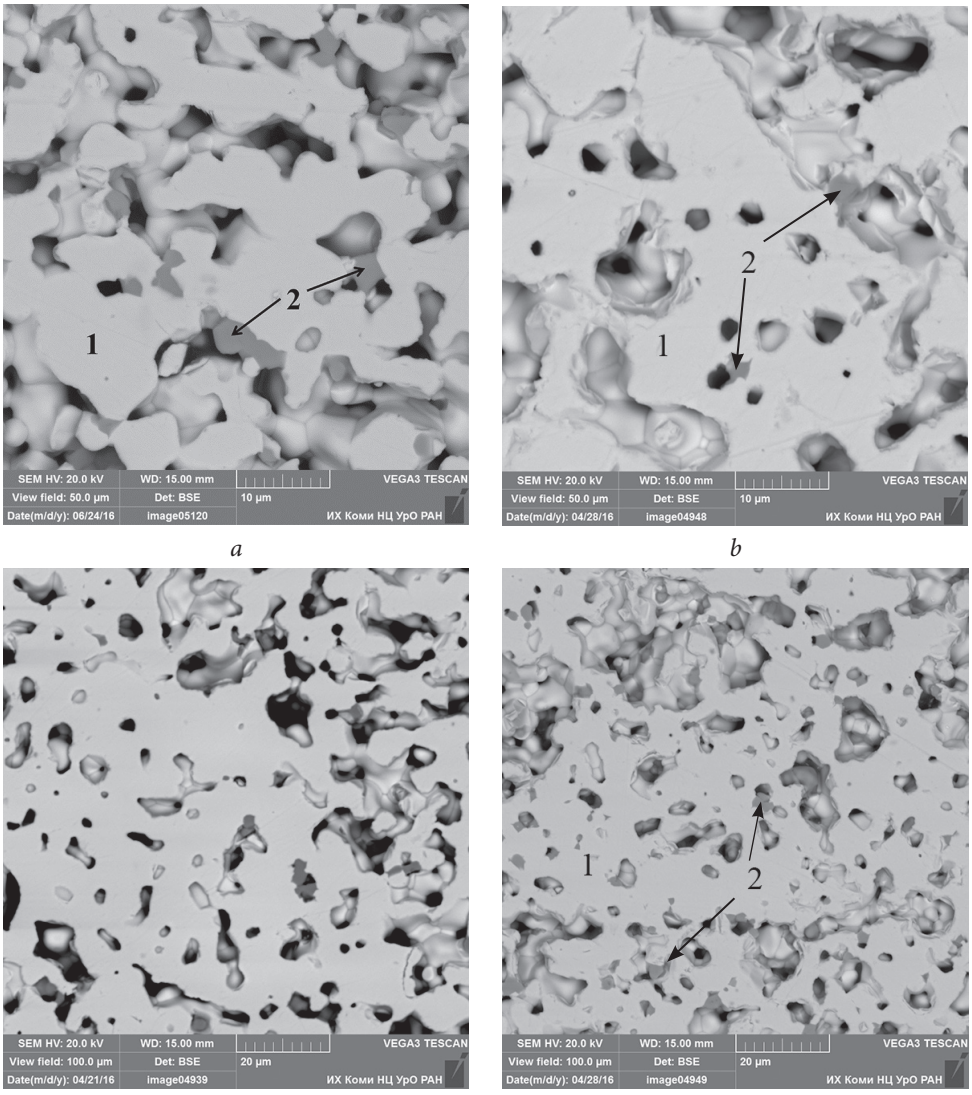

Fig. 2. SEM images of $Bi_{1.6}Mg_{0.8-x}Ni_xNb_{1.6}O_{7-\delta}$ samples: *a* – $x = 0$ (1 – $Bi_{1.72}Mg_{0.78}Nb_{1.6}O_{7-\delta}$, 2 – $MgNb_2O_6$); *b* – $x = 0.2$ (1 – $Bi_{1.60}Mg_{0.44}Ni_{0.18}Nb_{1.6}O_{7-\delta}$, 2 – $Mg_{0.85}Ni_{0.11}Nb_2O_6$); *c* – $x = 0.4$ ($Bi_{1.60}Mg_{0.38}Ni_{0.45}Nb_{1.6}O_{7-\delta}$); *d* – $x = 0.6$ (1 – $Bi_{1.68}Mg_{0.16}Ni_{0.56}Nb_{1.6}O_{7-\delta}$, 2 – $Mg_{0.35}Ni_{0.55}Nb_2O_6$)

to 96*h* sites) is observed. The observed, calculated and difference X-ray diffraction profiles for the model are shown in Fig. 4. To our mind, the distribution of dopant atoms in the cation sites is governed by the electronegativity values, apart from the ionic radii influence. So, Mg^{2+} and Ni^{2+} ionic radii are close (0.72 Å and 0.70 Å, respectively) [34]. The electronegativity of Mg (1.23) by Allred-Rochow [35] is equal to that of Nb (1.23), and the electronegativity of Ni (1.75) is close to that of Bi (1.67). Obviously, the electronegativity values impact on the dopant distribution in the pyrochlore structure, like in the Cu–Mg substituted bismuth niobates [28–29].

The pycnometric density of the $Bi_{1.6}Mg_{0.4}Ni_{0.4}Nb_{1.6}O_{7-\delta}$ powder is 6.50±0.24 g/cm³. The calculated density for the $[Bi_{1.56}M_{0.34}\square_{0.10}][M_{0.44}Nb_{1.56}]O_{7.02}$ model where M – the dopant metals (5% of vacancies in the Bi sites) is 7.02 g/cm³. The calculated density for the model with 18% vacancies in the Bi sites ($[Bi_{1.46}M_{0.18}\square_{0.36}][M_{0.54}Nb_{1.46}]O_{6.52}$) is 6.53 g/cm³ and is in agreement with the pycnometric density value. Thus assumed amount of about 15–20% vacant sites in Bi sublattice seems to be in agreement with the experimental results obtained in the present study.

Electrical properties

Complex impedance plots of the $Bi_{1.6}Mg_{0.8-x}Ni_xNb_{1.6}O_{7-\delta}$ ceramics were drawn from impedance spectroscopy data. The data were obtained during cooling from 700 to 160 °C to exclude proton conductivity. Perfect semicircles are traced in

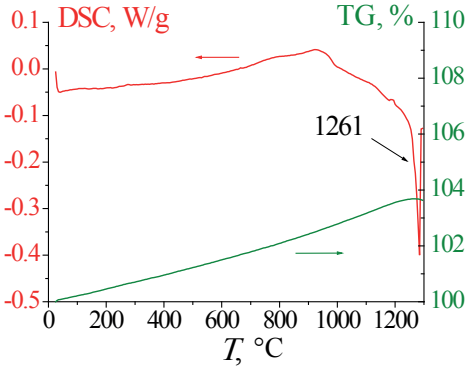

Fig. 3. DSC and TG curves of $Bi_{1.6}Mg_{0.4}Ni_{0.4}Nb_{1.6}O_{7-\delta}$

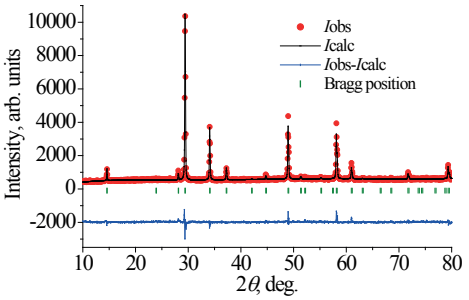

Fig. 4. Observed, calculated and difference X-ray diffraction profiles for $[Bi_{1.46}Ni_{0.18}\square_{0.36}][Ni_{0.18}Mg_{0.36}Nb_{1.46}]O_{6.52}$

Table 1

Refined crystallographic parameters for $Bi_{1.6}Mg_{0.4}Ni_{0.4}Nb_{1.6}O_{7-\delta}$ (space group *Fd*3*m*)

Atom type	Site	*x*	*y*	*z*	B_{iso}, Å²	Occupation
$[Bi_{1.46}Ni_{0.18}\square_{0.36}][Ni_{0.18}Mg_{0.36}Nb_{1.46}]O_{6.52}$						
Bi/Ni	96*h*	0	0.015	0.985	0.708	0.725/0.09
Nb/Ni	16*d*	1/2	1/2	1/2	0.003	0.725/0.09
Nb/Mg	16*d*	1/2	1/2	1/2	0.003	0.725/0.18
O	48*f*	1/8	1/8	0.428	0.010	1
O'	8*a*	1/8	1/8	1/2	0.010	0.52

a = 10.5204 Å; R_p = 4.51%, R_{wp} = 5.86%, χ^2 = 2.22.

the temperature range 320–700 °C. At the temperature less than 320 °C half semicircles may be observed. In Fig. 5 impedance plots for the $Bi_{1.6}Mg_{0.8-x}Ni_xNb_{1.6}O_{7-\delta}$ (x = 0.4; 0.6) ceramics are presented. The plots are well fitted by a single parallel RC element (inset of Fig. 5) where R and C belong to bulk resistance and capacitance, respectively [36–38]. The measured parameters are listed in Table 2.

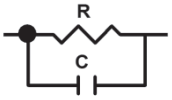

Permittivity recalculated from the capacitance values for the samples with Ni content x = 0.20, 0.40, and 0.60 is (70–81), (70–81), and (65–76), respectively, for the temperature range of 700–280 °C. Calculated permittivity does not depend on the frequency in the range of 1–1000 kHz and is close to the dc permittivity values. At room temperature, the permittivity is around 80 in the frequency range of 1–1000 kHz. All ceramics under investigation behave like a dielectric ($\tan\delta \approx 0.002$) up to 280 °C.

Calculated from Arrhenius direct conductivity plots activation energy values are close to 1.2 eV (the third column in Table 3). These values are almost equal to ones at 1 kHz (the second column in Table 3). The corresponding Arrhenius con-

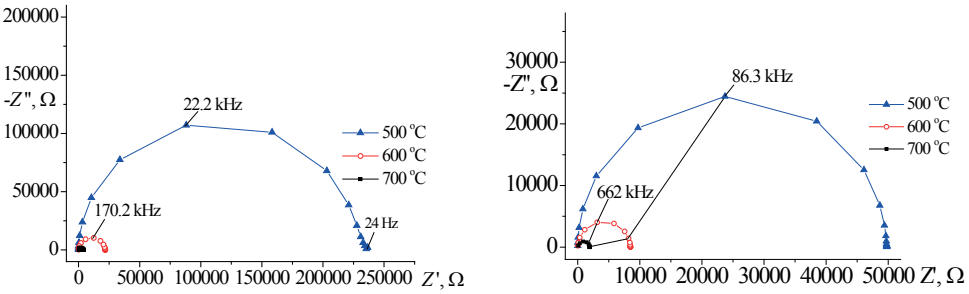

a *b*

Fig. 5. Complex impedance plots at 500, 600 and 700 °C for the $Bi_{1.6}Mg_{0.8-x}Ni_xNb_{1.6}O_{7-\delta}$ ceramics with x = 0.4; 0.6

Table 2

R_b and C_b parameters of the RC elements in the temperature range 280–700 °C for the $Bi_{1.6}Mg_{0.8-x}Ni_xNb_{1.6}O_{7-\delta}$ ceramics

T, °C	x = 0.20 (h = 0.265 cm; d = 1.280 cm)		x = 0.40 (h = 0.235 cm; d = 1.300 cm)		x = 0.60 (h = 0.220 cm; d = 1.325 cm)	
	R, kΩ	C, pF	R, kΩ	C, pF	R, kΩ	C, pF
280	$(79\pm3)\cdot10^4$	34.77±0.08	$(50\pm3)\cdot10^4$	40.61±0.18	$(111.7\pm2.7)\cdot10^3$	42.03±0.26
320	$(157.8\pm2.5)\cdot10^3$	34.32±0.11	–	–	$(173\pm3)\cdot10^2$	41.4±0.3
360	$(373\pm4)\cdot10^2$	33.99±0.15	$(310\pm4)\cdot10^2$	39.77±0.20	2860±30	40.8±0.3
400	9420±60	33.57±0.14	7560±40	39.18±0.12	606.8±2.4	39.97±0.15
500	558.5±2.3	32.41±0.14	164.4±0.5	37.87±0.12	49.61±0.08	38.66±0.09
600	62.8±0.4	31.08±0.28	21.52±0.04	36.57±0.13	8.460±0.014	37.36±0.14
700	8.972±0.026	29.88±0.19	4.032±0.010	35.22±0.24	1.913±0.004	35.8±0.3

ductivity plots at 1 kHz for all ceramics are shown in Fig. 6a. The activation energy values, which are greater than 1 eV, may be associated with ionic conduction. The same activation energy values (~1.27 eV) are known for the $(Bi_{1.5}Zn_{0.5})(Nb_{0.5}M_{1.5})O_7$ (M – Ti, Sn, Zr, and Ce) ceramics [19] at $T > 350$ °C with the ionic type of conductivity.

The conductivity dependences on the temperature for the $Bi_{1.6}Mg_{0.4}Ni_{0.4}Nb_{1.6}O_{7-\delta}$ ceramic (160–750 °C) in the air and in the oxygen atmosphere are shown in Fig. 6b. The conductivity of the ceramic does not dependent on the oxygen pressure, and the value of Seebeck coefficient is near 0 mV/K in the temperature range of 200–340 °C. These data indicate that there is no impurity-caused conductivity.

For all ceramics, an electrical modulus (M'') maximum is detected on the logarithmic scale of frequency (Fig. 7), indicating the presence of a polarization process. These relaxation effects are characterized by the full width at half maximum (FWHM) peaks of $M''(f)$ being ~ 1.2 decades. This value is close to an ideal Debye response (1.14 decades) that characterizes the ceramics as electrically homogenous. At frequencies of the M'' maximum value the relaxation time was calculated (Fig. 7). Frequency values at M'' maxima were plotted vs temperature in an Arrhenius-type fashion. Obtained accordingly values of activation energy are

Table 3

Activation energies of (dc, ac) conductivity and relaxation process of the substituted bismuth niobate pyrochlores

Compound	E_a (conductivity, 1 kHz), eV	E_a (conductivity, dc), eV	E_a (relaxation), eV
$Bi_{1.6}Mg_{0.8}Nb_{1.6}O_{7-\delta}$	1.03±0.06	–	–
$Bi_{1.6}Mg_{0.6}Ni_{0.2}Nb_{1.6}O_{7-\delta}$	1.09±0.03	1.25±0.03	1.38±0.03
$Bi_{1.6}Mg_{0.4}Ni_{0.4}Nb_{1.6}O_{7-\delta}$	1.14±0.03	1.20±0.03	1.38±0.03
$Bi_{1.6}Mg_{0.2}Ni_{0.6}Nb_{1.6}O_{7-\delta}$	1.10±0.03	1.20±0.04	1.23±0.04
$Bi_{1.6}Ni_{0.8}Nb_{1.6}O_{7-\delta}$	1.17±0.08	–	–

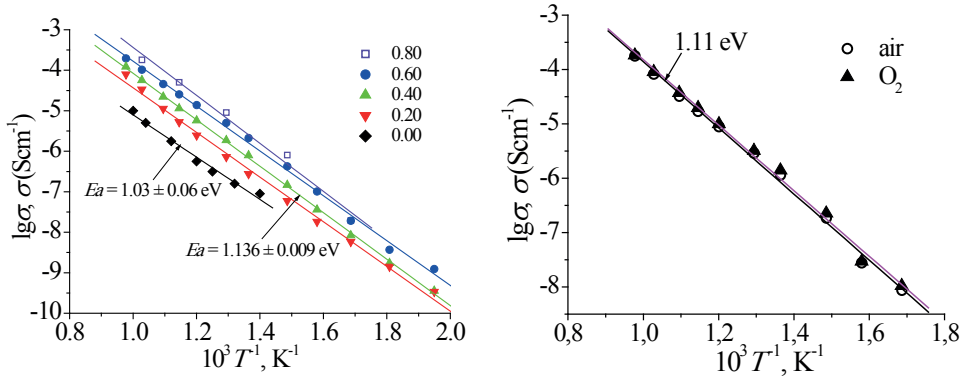

Fig. 6. Electrical conductivities as functions of reciprocal temperature at 1 kHz: *a* – $Bi_{1.6}Mg_{0.8-x}Ni_xNb_{1.6}O_{7-\delta}$; *b* – $Bi_{1.6}Mg_{0.4}Ni_{0.4}Nb_{1.6}O_{7-\delta}$

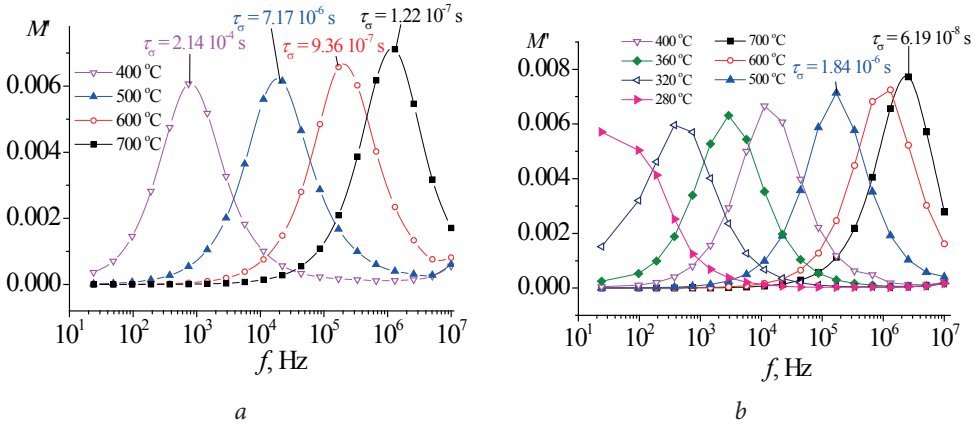

Fig. 7. Imaginary part of electrical modulus as a function of frequency for the $Bi_{1.6}Mg_{0.8-x}Ni_xNb_{1.6}O_{7-\delta}$ ceramics at $x = 0.4$ (*a*), $x = 0.6$ (*b*)

close to the ones obtained from the Arrhenius conductivity plots (Table 3). It points out that the hopping-type conductivity is typical for the $Bi_{1.6}Mg_{0.8-x}Ni_xNb_{1.6}O_{7-\delta}$ ceramics, like for $Bi_{1.5}ZnNb_{1.5}O_7$ [36, 38] and $Bi_{3.55}Mg_{1.78}Ta_{2.67}O_{13.78}$ [37] pyrochlores with E_a (relaxation) are 0.94 eV and 1.37 eV, respectively.

Conclusions

Mixed Mg–, Ni–containing bismuth niobates $Bi_{1.6}Mg_{0.8-x}Ni_xNb_{1.6}O_{7-\delta}$ ($0 \le x \le 0.8$) were synthesized by the conventional solid-state reaction method. For all samples the main crystal phase is the pyrochlore. The $Bi_{1.6}Mg_{0.4}Ni_{0.4}Nb_{1.6}O_{7-\delta}$ ceramic is a single-phase compound and is stable up to its melting point (1261 °C). Based on structural analysis and the comparison of pycnometric and calculated densities of the $Bi_{1.6}Mg_{0.4}Ni_{0.4}Nb_{1.6}O_{7-\delta}$, it was found that Mg atoms are distributed over the Nb sites, Ni atoms are distributed at the Bi and Nb sites almost in the equal ratio. In this case, there are about 15–20% vacant sites in the Bi sublattice. The $Bi_{1.6}Mg_{0.8-x}Ni_xNb_{1.6}O_{7-\delta}$ ceramics are characterized by the hopping type of conductivity (E_a = 1.0–1.4 eV). It was determined that dielectric permittivity varies from 81 to 65 as the temperature increases from 280 to 700 °C, and practically does not depend on frequency in the range of 1–1000 kHz.

Acknowledgements

This study received the financial support of Russian Foundation for Basic Research (project No. 15-03-09173 A). The study was performed using the equipment of the Center for Shared Use of Scientific Equipment "Khimiya" of the Institute of Chemistry, Komi Science Center, Ural Branch of the Russian Academy of Sciences.

References

1. Nino JC, Lanagan MT, Randall CA. Dielectric Relaxation in Bi_2O_3–ZnO–Nb_2O_5 Cubic Pyrochlore. *J Appl Phys.* 2001;89(8):4512–6. DOI:10.1063/1.1357468.

2. Liu W, Wang H. Enhanced dielectric properties of $Bi_{1.5}ZnNb_{1.5}O_7$ thick films via cold isostatic pressing. *J Electroceram.* 2012;29:183–6. DOI:10.1007/s10832-012-9758-8.
3. Ren W, Trolier-Mckinstry S, Randall CA, Shrout TR. Bismuth zinc niobate pyrochlore dielectric thin films for capacitive applications. *J Appl Phys.* 2001;89(1):767–74. DOI:10.1063/1.1328408.
4. Levin I, Amos TG, Nino JC, Vanderah TA, Randall CA, Lanagan MT. Structural Study of an Unusual Cubic Pyrochlore $Bi_{1.5}Zn_{0.92}Nb_{1.5}O_{6.92}$. *J Solid State Chem.* 2002:168:69–75. DOI:10.1006/jssc.2002.9681.
5. Jiang SW, Li YR, Li RG, Xiong ND, Tan LF, Liu XZ, Tao BW. Dielectric properties and tunability of cubic pyrochlore $Bi_{1.5}MgNb_{1.5}O_7$ thin films. *Appl Phys Lett.* 2009;94:162908-1-162908-3. DOI:10.1063/1.3126442.
6. Xia W, Xue P, Wu H, Lu Y, Zhang Y, Zhou Sh, Zhu X. Dielectric properties and atomic-scale microstructural characterizations of cubic-pyrochlored ceramics in the system of Bi_2O_3-MgO-Nb_2O_5. *J Alloys Compd.* 2017;701:682-8. doi:10.1016/j.jallcom.2017.01.153.
7. Gao L, Jiang Sh, Li R, Li B, Li Y. Structure and dielectric properties of sputtered bismuth magnesium niobate thin films. *Thin Solid Films.* 2012;520:6295-8. DOI:10.1016/j.tsf.2012.06.035.
8. Zhang Y, Zhu X, Zhou Sh, Zhu J, Liu Zh, Al-Kassab T. Atomic-scale microstructural characterization and dielectric properties of crystalline cubic pyrochlore $Bi_{1.5}MgNb_{1.5}O_7$ nanoparticles synthesized by sol–gel method. *J Nanopart Res.* 2014;16:2208. DOI:10.1007/s11051-013-2208-y.
9. Tan PY, Tan KB, Khaw CC, Zainal Z, Chen SK, Chon MP. Phase equilibria and dielectric properties of $Bi_{3+(5/2)x}Mg_{2-x}Nb_{3-(3/2)x}O_{14-x}$ cubic pyrochlores. *Ceramics International.* 2014;40:4237–46. DOI:10.1016/j.ceramint.2013.08.087.
10. Lufaso MW, Vanderah TA, Pazos IM, Levin I, Roth RS, Nino JC, Provenzano V, Schenck PK. Phase formation, crystal chemistry, and properties in the system Bi_2O_3–Fe_2O_3–Nb_2O_5. *J Solid State Chem.* 2006;179:3900–10. DOI:10.1016/j.jssc.2006.08.036.
11. Vanderah TA, Lufaso MW, Adler AU, Levin I, Nino JC, Provenzano V, Schenck PK. Subsolidus phase equilibria and properties in the system Bi_2O_3:$Mn_2O_{3\pm x}$:Nb_2O_5. *J Solid State Chem.* 2006;179:3467-3477. DOI: 10.1016/j.jssc.2006.07.014.
12. Sirotinkin VP, Bush AA. Preparation and Dielectric Properties of $Bi_{1.5}MNb_{1.5}O_7$ (M = Cu, Mg, Mn, Ni, Zn) Pyrochlore Oxides. *Inorg Mater.* 2003;39(9):974–7. DOI:10.1023/A:1025517507623.
13. Vanderah TA, Siegrist T, Lufaso MW, Yeager MC, Roth RS, Nino JC, Yates S. Phase formation and properties in the system Bi_2O_3: $2CoO_{1+x}$:Nb_2O_5. *Eur J Inorg Chem.* 2006;23:4908–14. DOI:10.1002/ejic.200600661.
14. Nguyen HB, Norèn L, Liu Y, Withers RL, Wei X, Elcombe MM. The disordered structures and low temperature dielectric relaxation properties of two misplaced-displacive cubic pyrochlores found in the Bi_2O_3–$M^{II}O$–Nb_2O_5 (M = Mg, Ni) systems. *J Solid State Chem.* 2007;180:2558–65. DOI:10.1016/j.jssc.2007.07.003.

15. Nguyen B, Liu Y, Withers RL. The local crystal chemistry and dielectric properties of the cubic pyrochlore phase in the Bi_2O_3–$M^{2+}O$–Nb_2O_5 (M^{2+} – Ni^{2+} and Mg^{2+}) systems. *J Solid State Chem.* 2007;180:549–57. DOI:10.1016/j.jssc.2006.10.039.
16. Li LX, Zhang S, Lv XS. Crystal chemistry and dielectric properties of $(Bi_{1.5}Zn_{0.4}M_{0.1})(Nb_{1.5}Zn_{0.5})O_7$ (M = Sr, Ca, Mn, Zn) pyrochlore oxides. *J Mater Sci: Mater Electron.* 2017;28(5):4388-95. DOI:10.1007/s10854-016-6066-0.
17. Shihua D, Yong P, Tianxiu S, Hongni W, Peng X, Lihua Y. Dielectric Properties of Ca Doping a-BZN Ceramics. *Ferroelectrics.* 2015;487:161–7. DOI:10.1080/00150193.2015.1071628
18. Luo W, Li L, Guo Q, Lv X. Crystal structure and dielectric properties of Mn-substituted $Bi_{1.5}Zn_{1.0}Nb_{1.5}O_7$ pyrochlore ceramics as temperature stable LTCC material. *J Mater Sci: Mater Electron.* 2017;28:5623–7. DOI:10.1007/s10854-016-6232-4.
19. Du H, Shi X, Cui Y. Defect structure and electrical conduction behavior of Bi-based pyrochlores. *Solid State Commun.* 2010;150:1213–6. DOI:10.1016/j.ssc.2010.04.008.
20. Osman RAM, West AR. Electrical characterization and equivalent circuit analysis of $(Bi_{1.5}Zn_{0.5})(Nb_{0.5}Ti_{1.5})O_7$ Pyrochlore, a relaxor ceramic. *J Appl Phys.* 2011;109:074106-1-074106-8. DOI:10.1063/1.3553883.
21. Valant M, Davies PK. Crystal Chemistry and Dielectric Properties of Chemically Substituted $(Bi_{1.5}Zn_{1.0}Nb_{1.5})O_7$ and $Bi_2(Zn_{2/3}Nb_{4/3})O_7$ Pyrochlores. *J Am Ceram Soc.* 2000;83(1):147–53. DOI:10.1111/j.1151-2916.2000.tb01163.x.
22. Du H, Yao X, Wang H. Dielectric properties of pyrochlore $(Bi_{1.5}Zn_{0.5})(Nb_{0.5}M_{1.5})O_7$ (M = Ti, Sn, Zr, and Ce) dielectrics. *Appl Phys Lett.* 2006;88:212901-1-212901-3. DOI:10.1063/1.2200480.
23. Qasrawi AF, Mergen A. Structural, electrical and dielectric properties of $Bi_{1.5}Zn_{0.92}Nb_{1.5-x}Ta_xO_{6.92}$ pyrochlore ceramics. *Ceramics International.* 2012;38:581–7. DOI:10.1016/j.ceramint.2011.07.046.
24. Wang H, Zhang D, Wang X, Yao X. Effect of La_2O_3 Substitution on Structure and Dielectric Properties of Bi_2O_3–ZnO–Nb_2O_5-based Pyrochlore Ceramics. *J Mater Res.* 1999;14(2):546–8. DOI:10.1557/JMR.1999.0078.
25. Dasin NAM, Tan KB, Khaw CC, Zainal Z, Chen SK. Subsolidus solution and electrical properties of Sr-substituted bismuth magnesium niobate pyrochlores. *Ceramics International.* 2017;43:10183–91. DOI:10.1016/j.ceramint.2017.05.043.
26. Huang B, Liu Y, Lu Y, Gao H, Chen H. Structure and dielectric properties of Nd substituted $Bi_{1.5}MgNb_{1.5}O_7$ ceramics. *J Mater Sci: Mater Electron.* 2013;24:2785–9. DOI:10.1007/s10854-013-1171-9.
27. Ning P-F, Li L-X, Xia W-S, Zhang X-Y. Low temperature crystallized voltage tunable $Bi_{1.5}Cu_xMg_{1-x}Nb_{1.5}O_7$ thin films capable of integration with Au electrode. *Ceramics International.* 2012;38:5299–303. DOI:10.1016/j.ceramint.2012.02.088.
28. Koroleva MS, Piir IV, Sekushin NA. Mg-Ni and Mg-Cu containing bismuth niobates: synthesis, structure and electrical properties. In: Articles of the 21h International Conference Solid State Ionics; 2017 June 18-23; Padua, Italy. p. 357.
29. Koroleva MS, Piir IV, Sekushin NA, Istomina EI. Sintez i elektricheskie svoystva magniy-med'-, magniy-nikel'soderzhashchikh niobatov vismuta [Synthesis and electrical properties of magnesium-copper, magnesium-nickel-containing bismuth

niobates]. In: Articles of the First International Conference on Intellect-intensive technologies in power engineering (physical chemistry and electrochemistry of molten and solid state electrolytes); 2017 Sep 18-22; Ekaterinburg, Russia. P. 363–365. Russian.
30. Withers RL, Welberry TR, Larsson A-K, Liu Y, Norén L, Rundlöf H, Brink FJ. Local crystal chemistry, induced strain and short range order in the cubic pyrochlore $(Bi_{1.5-\alpha}Zn_{0.5-\beta})(Zn_{0.5-\gamma}Nb_{1.5-\delta})O_{(7-1.5\alpha-\beta-\gamma-2.5\delta)}$ (BZN). *J Solid State Chem.* 2004;177(1):231–44. DOI:10.1016/j.jssc.2003.07.005
31. Piir IV, Koroleva MS, Ryabkov YuI, Pikalova EYu, Nekipelov SV, Sivkov VN, Vyalikh DV. Chemistry, structure and properties of bismuth copper titanate pyrochlores. *Solid State Ionics.* 2014;262:630–5. DOI:10.1016/j.ssi.2013.08.041.
32. Krasnov AG, Piir IV, Koroleva MS, Sekushin NA, Ryabkov YI, Piskaykina MM, Sadykov VA, Sadovskaya EM, Pelipenko VV, Eremeev NF. The conductivity and ionic transport of doped bismuth titanate pyrochlore $Bi_{1.6}M_xTi_2O_{7-\delta}$ (M – Mg, Sc, Cu). *Solid State Ionics.* 2017;302:118–25. DOI:10.1016/j.ssi.2016.12.019.
33. Rodríguez-Carvajal J. Recent advances inmagnetic structure determination by neutron powder diffraction. *Phys B Condens Matter.* 1993;192:55–69. DOI:10.1016/0921-4526(93)90108-I.
34. Shannon RD. Revised effective ionic radii and systematic studies of interatomic distances in halides and chalcogenides. *Acta Cryst.* 1976;A32:751–67. DOI:10.1107/S0567739476001551.
35. Allred AL, Rochow EG. A scale of electronegativity based on electrostatic force. *J Inorg Nucl Chem.* 1958;5(4):264–8. DOI:10.1016/0022-1902(58)80003-2.
36. Singh J, Krupanidhi SB. Probing disorder in cubic pyrochlore $Bi_{1.5}Zn_{1.0}Nb_{1.5}O_7$ (BZN) thin films. *Solid State Commun.* 2010;150:2257–61. DOI:10.1016/j.ssc.2010.09.030.
37. Tan PY, Tan KB, Khaw CC, Zainal Z, Chen SK, Chon MP. Structural and electrical properties of bismuth magnesium tantalate pyrochlores. *Ceramics International.* 2012;38(7):5401-9. DOI:10.1016/j.ceramint.2012.03.050.
38. Tan KB, Khaw CC, Lee CK, Zainal Z, Tan YP, Shaari H. High temperature impedance spectroscopy study of non-stoichiometric bismuth zinc niobate pyrochlore. *Mater Sci Pol.* 2009;27:947–59. Available from: http://www.materialsscience.pwr.wroc.pl/

Cite this article as:
Koroleva MS, Piir IV, Istomina EI. Synthesis, structure and electrical properties of Mg-, Ni-codoped bismuth niobates. *Chimica Techno Acta*. 2017;4(4):231–41. DOI:10.15826/chimtech/2017.4.4.04.